THE UNIVERSITY of EDINBURGH

Edinburgh Research Explorer

Photocatalytic treatment of saccharin and bisphenol-A in the presence of TiO2 nanocomposites tuned by Sn(IV)

Citation for published version:
Davididou, K, Hale, E, Lane, N, Chatzisymeon, E, Pichavant, A & Hochepied, J-F 2017, 'Photocatalytic treatment of saccharin and bisphenol-A in the presence of TiO2 nanocomposites tuned by Sn(IV)', *Catalysis today*. https://doi.org/10.1016/j.cattod.2017.01.038

Digital Object Identifier (DOI):
10.1016/j.cattod.2017.01.038

Link:
Link to publication record in Edinburgh Research Explorer

Document Version:
Peer reviewed version

Published In:
Catalysis today

General rights
Copyright for the publications made accessible via the Edinburgh Research Explorer is retained by the author(s) and / or other copyright owners and it is a condition of accessing these publications that users recognise and abide by the legal requirements associated with these rights.

Take down policy
The University of Edinburgh has made every reasonable effort to ensure that Edinburgh Research Explorer content complies with UK legislation. If you believe that the public display of this file breaches copyright please contact openaccess@ed.ac.uk providing details, and we will remove access to the work immediately and investigate your claim.

Download date: 16. Mar. 2025

Photocatalytic treatment of saccharin and bisphenol-A in the presence of TiO_2 nanocomposites tuned by Sn(IV)

K. Davididou[1], E. Hale[1], N. Lane[1], E. Chatzisymeon[1*], A. Pichavant[2,3], J.-F. Hochepied[2,3]

(1) Institute for Infrastructure and Environment, School of Engineering, The University of Edinburgh, Edinburgh EH9 3JL, United Kingdom.

(2) MINES ParisTech, PSL Research University, Centre des Matériaux, BP87 91003 Evry, France.

(3) ENSTA ParisTech, Unité Chimie et Procédés, 828 Bd des Maréchaux, 91762 Palaiseau Cedex, France.

*Corresponding author: E-mail: e.chatzisymeon@ed.ac.uk; Tel.: +44 1316505711

Abstract

This study deals with the photocatalytic treatment of saccharin (SAC) and bisphenol-A (BPA) under UV irradiation. For this purpose, novel submicronic anatase–rutile nanocomposite particles with tuned phase ratio produced by thermohydrolysis of acidic Ti(IV) solutions in the presence of controlled amounts of Sn(IV) were used. These catalysts were then assessed regarding their efficiency to degrade SAC or BPA, which are contaminants of increased environmental and health concern. The effect of various operating conditions, such as the anatase-rutile ratio (100:0, 85:15, 70:30), catalyst concentration (50-600 mg/L) and solute concentration (3-10 mg/L) was investigated. Furthermore, catalyst reuse -an important but little studied aspect- was assessed. Anatase–rutile nanocomposites were successfully prepared presenting good crystallinity and surface quality. Their activity was about the same for removing SAC or BPA from water. It was found that photocatalytic performance was increased with catalyst loading up to 400 mg/L. A further increase to 600 mg/L did not significantly enhance BPA removal, thus associating this tendency with screening effects. Also, photocatalytic efficiency was increased with initial solute concentration decrease. Organics degradation followed a pseudo-first order kinetic rate in terms of both SAC and BPA removal. The reproducibility of catalyst activity was assessed in three successive reuse cycles, where the removal percentage of initially 5 mg/L SAC was maintained as high as 70% at the end of the 3rd cycle, in the presence of initially 400 mg/L anatase catalyst, and after 90 min of treatment. Finally, additional experimental runs were carried out with ultrasound cleaning (US) being applied to the reactant mixture at the beginning of each reuse cycle, but it was found to have no significant effect on treatment efficiency.

Keywords: photocatalysis; catalyst recovery; thermohydrolysis; titania nanostructures; endocrine disruptors; artificial sweeteners

1 Introduction

Endocrine disrupting compounds (EDCs) are chemicals with documented estrogenic or androgenic activity, at trace-level concentrations, that pose serious threats to human health and wildlife [1, 2]. Various chemicals have been identified as potential EDCs including pharmaceuticals, personal care products, pesticides and herbicides, industrial chemicals, heavy metals and recently artificial sweeteners (ASs) [3-5]. ASs are metabolically inert sugar substitutes, being used increasingly in food, beverages and pharmaceuticals [6, 7], which eventually end up in domestic sewage treatment plants (STPs) mainly unchanged [8, 9]. Among them, saccharin (SAC), the forerunner of ASs, has been identified in STP effluents, rivers, and groundwater aquifers [8-10], thus reflecting the inefficiency of conventional wastewater treatment processes in eliminating recalcitrant organic compounds [3, 11]. Another critical issue related to ASs is the elevation of toxicity and the production of by-products more persistent than the parent compounds during their natural attenuation [3, 12, 13]. Furthermore, bisphenol-A (BPA) is also included among the widely detectable organic xenobiotics in urban wastewaters and treated effluents [5]. BPA is used extensively in the production of polycarbonate polymers and epoxy resins and its occurrence in waterways is an emerging environmental issue since its endocrine disruption has been well documented [14]. The major routes of EDCs in the aquatic environment are via municipal and industrial STP effluent discharges [4, 5, 15]. Therefore, the current focus is on the identification of new efficient methods able to mineralise persistent organic compounds, such as SAC and BPA, and hence preventing their discharge into the environment.

Heterogeneous photocatalysis is an advanced oxidation process (AOP) that has received considerable attention in this direction as its efficiency to eliminate persistent organic compounds has been well proved [16, 17]. Photocatalytic oxidation is initiated upon UV illumination of a semiconductor catalyst, for example TiO_2 [14, 16]. Highly reactive species, mainly hydroxyl radicals (•OH), are then formed, which can attack organic pollutants until their final mineralisation into CO_2 and inorganic anions [16, 18]. Anatase TiO_2 is a widely used photocatalyst, due to its low cost and good performance, for many applications [18]. A way to enhance its photocatalytic activity is to improve the charge separation and migration to the catalyst surface by means of interfaces with semiconductor or metallic particles. In addition to material modification, the control of nano-architecture and morphology is another way to enhance catalyst performance [19]. Therefore, a combination of these two levers (i.e. creating interfaces between anatase and rutile polymorphs) could be a key asset to improve photocatalytic performance. In general,

62 homogeneous precipitation by thermohydrolysis of acidic Ti(IV) precursors is an easy way to produce titania
63 nanoparticles, yet the control of anatase–rutile ratio is rather difficult to master and is very sensitive to
64 physicochemical conditions [19]. To get anatase–rutile interfaces, co-precipitating anatase and rutile in one pot by
65 thermohydrolysis can, therefore, be a challenging task, especially if one wants to tune anatase:rutile ratio with
66 small and controlled amounts of metals that act as rutile phase promoters. In this work a direct approach, just by
67 hydrolysing as-received commercial products without additives nor surfactants, is proposed in order to produce
68 interfaced anatase-rutile photocatalysts tuned by Sn(IV).
69 It should be highlighted that the photocatalytic treatment of ASs, such as saccharin, acesulfame and sucralose,
70 has only recently started to be studied [3, 12, 13, 20]. To the best of our knowledge, only Chen et al. (2014) deal
71 with the photocatalytic degradation of SAC [21]. Specifically, they observed 93% TOC removal in the presence of
72 0.8 g/L Degussa P25, after 3 hr irradiation under a 500 W mercury lamp. Also, they found that the reaction followed
73 pseudo-first-order degradation. However, the investigation of the optimal operating parameters of a UV/TiO_2
74 system as described in this paper still remains a missing element in literature.
75 The overall aim of this work was to investigate the photocatalytic degradation of SAC and BPA, as contaminants
76 of emerging environmental and health concern, in the presence of novel interfaced anatase-rutile catalysts
77 produced by thermohydrolysis and tuned by Sn(IV). These catalysts showed promising photocatalytic activity for
78 phenol removal [19] and for this reason they were also employed for SAC and BPA treatment. In view of this, the
79 effect of key operating parameters, such as initial solute concentration, catalyst type, catalyst concentration and
80 reuse, on photocatalytic performance was assessed. Finally, the effect of ultrasound cleaning on catalytic activity
81 was evaluated.
82

83 **2 Materials and methods**

84 *2.1 Chemicals*

85 All chemicals used in this study were of analytical grade and without further modification. SAC (CAS No: 81-07-2)
86 and BPA (CAS No: 80-05-7) were purchased from Acros and Sigma-Aldrich, respectively. $TiOSO_4.xH_2O$ (CAS
87 13825-74-6), $SnCl_4.5H_2O$ (CAS 10026-06-9) and H_2SO_4 (CAS 7664-93-9) were supplied by Sigma-Aldrich.

Aeroxide TiO_2 P25 (P25) obtained from Evonik Industries, KRONOClean 7050 (KR7050) from KRONOS Worldwide, Inc. and CristalACTiV PC105 (PC105) from CRISTAL were also used.

2.2 Catalyst preparation

Syntheses of anatase-rutile composites were performed according to previously published protocol [19], where low quantities of Sn(IV) were used as rutile phase promoter. Pichavant et al. (2014) [19] found that rutile phase ranging between X_R=0.15-0.3 led to the highest photocatalytic removal of phenol. Given this, R30 was the highest rutile fraction to be used in the present work. In detail, $TiOSO_4.xH_2O$ and $SnCl_4.5H_2O$ were dissolved in distilled water acidified with H_2SO_4 so that the total concentration [Ti(IV)]+[Sn(IV)] was 1.5 mol/L and the total sulphate concentration was 2 mol/L. The quantity of Sn introduced, X_{Sn}=[Sn(IV)]/([Ti(IV)]+[Sn(IV)]), was 0, $1.7x10^{-3}$ and $6.8x10^{-3}$ mol/L, for pure anatase (ANA), 15% rutile (R15) and 30% rutile (R30) catalyst samples, respectively. The obtained transparent solutions were transferred into Teflon vials and heated in a microwave oven (Synthos 3000, Anton Paar), without stirring, following a ramp from room temperature to 120°C at 5°C/min, reaching a plateau at 120°C for 1 h and finally returning to room temperature at approx. -5°C/min. The white precipitates were washed by successive centrifugation/redispersion in water. Powders were finally obtained by freeze-drying.

2.3 Catalyst characterization techniques

X-ray diffractograms were obtained by a Bruker D8 using Co $K\alpha_1$ radiation, λ = 1,789 Å and a scintillation counter. The rutile ratio was calculated according to the law $X_R = I_R(110)/((0.884*I_A(101)+ I_R(110))$ [22], $I_R(110)$ being the integrated intensity of rutile (110) peak and $I_A(101)$ the integrated intensity of anatase (101) peak, after signal deconvolution. Specific surface area was measured by nitrogen gas adsorption at 77K with an ASAP2000 instrument from Micromeritics. Transmission Electron Microscopy (TEM) was performed on a TECNAI 20F.

2.4 Photocatalytic experiments

Experiments were conducted in an immersion well, batch operating photoreactor applying a working volume of 500 mL. UV irradiation was provided by an 11W low-pressure blacklight fluorescent lamp (PLS G23, Casell Lighting) emitting predominantly at 365 nm. The photon flux emission of the lamp was determined by potassium ferrioxalate actinometer, as described by Murov et al. [23], and found to be 4.98 x 10^{-6} Einstein/s.

In a typical run, SAC or BPA solution was loaded in the photoreactor and the appropriate amount of catalyst was added. The slurry solution in the reactor was continuously magnetically stirred to promote uniform dispersion of catalyst powder and dissolved oxygen. At the beginning of each experiment, the solution was stirred in the dark for 30 min to obtain adsorption-desorption equilibrium of organic pollutants onto the catalyst surface. The lamp was then switched on and at regular time intervals, samples were withdrawn and filtered through 0.45 μm syringe filters and further analysed in terms of their organic content. All the experiments were conducted at room temperature (i.e. 22 ^{o}C) and natural pH of SAC and BPA solutions (~ 4.6 and 6.4 for SAC and BPA, respectively). Also, during all experimental runs, the photocatalytic set-up was covered with aluminium foil to prevent irradiation losses and to minimise penetration of ambient light.

2.5 Analytical techniques

BPA or SAC concentration in filtrate samples was measured by means of a high performance liquid chromatography (HPLC) system (S200 Pump, S225 Autosampler, Perkin Elmer) coupled with a diode array detector (S200 EP, Perkin Elmer). Samples were separated by reverse phase (RP) chromatography using a C18 Luna (Phenomenex) column (5u, 250 x 4.6 mm). HPLC method for SAC was obtained from Trandafil et al. (2009) [24] and was appropriately modified. The mobile phase consisted of 85 vol.% 0.02 M KH_2PO_4 and 15 vol.% CH_3CN fed at a flow rate of 1 mL/min. The elution was isocratic and the injection volume was 40 μL. The detection wavelength was at λ=216 nm. BPA concentration was measured by HPLC method obtained by Daskalaki et al. (2011) [25] at a wavelength of 225 nm. The mobile phase was a mixture of water/acetonitrile (35/65, v/v) at a flow rate of 1 mL/min. The solvents were eluted isocratically and the injection volume was kept at 40 μL.

The degree of SAC and BPA photomineralisation was determined by measuring the residual organic concentration by a TOC analyser (Shimadzu TOC-V_{CPH}).

2.6 Catalyst recovery and reuse

Experiments were carried out to assess the photocatalytic activity of the prepared catalysts after three successive photocatalytic runs. Catalyst recovery was performed at the end of the each cycle, after centrifuging the reactant mixture, to separate catalyst particles from the supernatant effluent. The obtained TiO_2 precipitate was then reused,

as the catalyst, for the successive photocatalytic run. The effect of sonication on catalytic performance was also investigated by placing, at the beginning of each cycle, the reactant mixture into an ultrasound bath for 10 min.

3 Results and Discussion

3.1 Catalyst characterization

The specific surface area of the pure anatase (ANA), 15% rutile (R15) and 30% rutile (R30) catalyst samples was 197, 201, and 172 m^2/g, respectively, with the corresponding equivalent spherical diameters being 7.8, 7.6, and 8.9 nm. These relatively small particle sizes suggest a low particle growth step after nucleation during thermohydrolysis with well-crystallised particles, contrary to other methods requiring calcination. XRD characterizations for the produced TiO_2 nanocomposites are shown in Figure 1, where it is clear that Ti(IV) thermohydrolysis in sulphuric medium yields pure anatase particles. Furthermore, the R15 and R30 samples, mentioned in this Figure, show that the incorporation of a small amount of Sn^{4+} in the crystal lattice is sufficient to induce considerable rutile crystallisation. Indeed, XRD measurements indicate not only remaining anatase crystallisation but also rutile crystallisation revealed by the (110), (101) and (111) peaks' emergence. Moreover, no peak indicating SnO_2 crystallisation is observed, bearing out that Sn^{4+} ions are incorporated into TiO_2 lattice inducing rutile crystallisation.

Figure 1

Finally, TEM observations shown in Figure 2 indicate that nanocrystals are much agglomerated and form spherical substructures of around 100 nm size. In addition to the specific surface area values, these observations suggest that the synthesised structures are porous agglomerates. At higher magnification, it can be seen that reticular plans are very oriented between neighbour nanocrystals.

Figure 2

3.2 Evaluation of photocatalytic activity

To evaluate the relative activity of the prepared catalysts ANA, R15 and R30, preliminary experiments were carried out at 5 mg/L SAC or BPA initial concentration and 50 mg/L catalyst loading. In addition, experiments were performed in the presence of P25, KR7050 and PC105 photocatalysts, at the same operating conditions, to establish a comparison against commercially available catalysts. It was observed that the highest SAC and BPA removal (i.e. 98% and 99%, respectively) was obtained when P25 was used as the catalyst. 67% and 38% of SAC and BPA, respectively, was removed in the presence of PC105, whereas KR7050 resulted in 43% degradation of both organics within 90 min of photocatalytic treatment (data not shown). On the other hand, the three prepared catalysts, namely ANA, R15 and R30, yielded similar efficiencies with each other (Figure 3). Specifically, their performance ranged from 21 to 27% and from 22 to 25% in terms of SAC and BPA removal, respectively, indicating that, under these experimental conditions, anatase–rutile interfaces do not affect SAC or BPA degradation. However, as shown in our previous study, where the photocatalytic degradation of phenol in the presence of such catalysts was examined, it was found that anatase–rutile interfaces could affect process efficiency [19]. Specifically, total phenol (with C_0=7.5 mg/L) degradation was achieved in the presence of 400 mg/L of 15% rutile and after about 90 min of treatment, while phenol degradation was about 75% and 80% in the presence of pure anatase and 30% rutile, respectively. Also, Fresno et al. (2009) investigated the gas-phase photocatalytic degradation of trichloroethylene activity in the presence of $Ti_{1-x}Sn_xO_2$ catalysts. They observed a beneficial effect of Sn^{4+} in the activity of TiO_2 which was related to the formation of anatase–rutile mixtures, leading to the highest photocatalytic activity in the sample of composition $Ti_{0.93}Sn_{0.07}O_2$, with anatase:rutile ratio close to 3 [26].

Furthermore, experiments were carried out in the dark to assess the adsorption capacity of ANA, R15, R30 and P25 catalysts and results are shown in Figure 3. It was observed that there is no correlation between the adsorption capacity and the corresponding photocatalytic activity, under the experimental conditions applied. For instance, P25, which led to the highest photocatalytic removal of both organics, interestingly yielded very low adsorption capacity (i.e. 3% for BPA and 0.8% for SAC) that was almost the same with that of the ANA, R15, and R30 catalysts. Moreover, BPA was found to be adsorbed slightly greater than SAC onto catalyst surface, result that may be ascribed to the different size of the two organics (BPA 228.29 g/mol, SAC 183.18 g/mol), given that all other experimental parameters were identical. It has been previously reported that adsorption of organic substances onto catalytic surface increases with the molecular weight [27], thus explaining the obtained results.

Considering the above findings and previously published works, which encourage the use of such type of materials as photocatalysts, we decided to proceed with further experiments, to optimise the process and explore the capacity of these catalysts to eliminate SAC or BPA.

Figure 3

3.3 Effect of the initial solute concentration

Initial SAC or BPA concentration, in the range of 3-10 mg/L, was applied, in the presence of 400 mg/L ANA or R30 respectively, to evaluate the effect of initial solute concentration on photocatalytic performance. In Figures 4 and 5, it becomes apparent that the increase in the initial organic concentration, at a given catalyst loading, leads to decreased removal efficiency. Specifically, the increase of SAC concentration from 3 to 10 mg/L resulted in the gradual removal decrease from 88% to 52% (Figure 4). Similarly, the BPA conversion rate decreased progressively from 48% to 17% when the initial BPA load increased from 3 to 10 mg/L (Figure 5). In both cases, the results were found to approach well the pseudo-first order reaction model. Plots of the logarithm of normalised SAC and BPA concentration against time resulted in straight lines with the coefficient of linear regression of data fitting, r^2, ranging from 98 to 99% and from 94 to 99% for SAC and BPA, respectively (data not shown). In addition, there is an almost linear relationship between the rate constant, k, and the initial solute concentration as can be seen in the inset graphs of Figures 4 and 5. For example, regarding BPA photocatalytic degradation when its initial concentration is doubled (e.g. from 5 mg/L to 10 mg/L) then the reaction rate constant is decreased by almost two times from 0.0049 min^{-1} to 0.0026 min^{-1}. At a fixed catalyst loading, efficiency is dictated by the catalyst active sites to organic molecules ratio. In other words, at relatively low solute loading the active sites provided by the semiconductor are in excess and can uptake most of the organic molecules, thus resulting in higher removal rates. The increase of the initial SAC or BPA concentration results in saturation of the limited catalyst surface by the organic molecules and their reaction by-products that further affects the photonic efficiency and subsequently the degradation rates, thus explaining the above findings [25].

Several studies have demonstrated the evolution of toxic intermediates during the photocatalytic treatment of EDCs [12, 28]. Calza et al. (2013) evaluated the ecotoxicity of sucralose solutions treated by heterogeneous photocatalysis [12]. They have observed that toxicity increases during treatment due to the formation of

intermediate compounds more toxic than sucralose. Similarly, Kondrakov et al. (2004) studied the TiO_2 photocatalytic degradation of BPA during which they identified potentially genotoxic by-products [28]. In this direction, SAC and BPA mineralization was monitored, at the best conditions assayed (i.e. C_0=3 mg/L and catalyst concentration=400 mg/L), to get an indication regarding the formation of potentially hazardous by-products. Results showed that, the organic content was decreased by 54 and 43% after 90 min of SAC and BPA photocatalytic treatment, respectively. SAC mineralisation was slightly faster than BPA following the same degradation profile with the parent compounds (i.e. SAC or BPA). Nonetheless, discrepancies between the concentration of TOC and parent compounds were observed. Specifically, SAC degradation was 88% while TOC removal was only 54% after 90 min of treatment. Similarly, when BPA degradation was 48%, TOC was removed by 43%. These discrepancies indicate the formation of organic by-products during treatment.

Figure 4

Figure 5

3.4 Effect of catalyst loading

To investigate the effect of catalyst loading on process efficiency, several TiO_2 concentrations (i.e. 50, 200, 400 and 600 mg/L) were examined for the photocatalytic degradation of 5 mg/L SAC or BPA concentration. As seen in Figure 6, although SAC degradation increased considerably with catalyst mass, this was not the case for BPA. In detail, SAC removal was 27%, 59%, 81% and 97% in the presence of 50, 200, 400 and 600 mg/L of ANA catalyst, respectively, and thus process efficiency was increased by about 70% when catalyst concentration was increased from 50 to 600 mg/L (Figure 6a). Furthermore, there is a linear relationship between the rate constant, k, and the catalyst concentration, where the increase of ANA in the range of 50-600 mg/L results in *k* increase from 0.0034 to 0.0238 min^{-1} (inset graph of Figure 6a). These results are explained by the fact that at higher amounts of TiO_2 (i.e. surface area), the increased number of active sites results in higher photogeneration rate of oxidising species, responsible for the photocatalytic oxidation [16]. Likewise, the same trend was followed during BPA degradation; the increase of R30 from 50 to 400 mg/L led to a 12% increase of process efficiency (Figure 6b). Nonetheless, further increase of R30 from 400 to 600 mg/L did not improve the photocatalytic performance, as can be seen in

Figure 6b. This is due to the fact that catalyst loading above a certain point, which seems to be around 400 mg/L for BPA, is associated with screening effects, the excessive TiO_2 particles mask the photosensitive active sites, and the removal efficiency becomes independent of the catalyst mass [16]. The effect of catalyst overloading on BPA photocatalytic treatment can also be seen in the inset graph of Figure 6b, where the rate constant, *k*, increases linearly from 0.0025 to 0.0049 min^{-1} up to 400 mg/L catalyst concentration. However, *k* remains almost the same (i.e. 0.0053 min^{-1}) with a further TiO_2 increase to 600 mg/L.

Figure 6

3.5 Effect of catalyst reuse

Catalyst recovery and reuse may be a good practice to reduce the operational cost of photocatalysis and hence to promote its competitiveness among other processes for water and wastewater treatment [29]. Considering this, ANA catalyst was subjected to three successive reuse cycles to determine its effectiveness for SAC treatment and the results are presented in Figure 7. It can be observed that the performance was kept stable during the 1st and 2nd cycle with SAC removal being 81% and 84%, respectively. Nonetheless, the catalyst effectiveness dropped to 70% at the 3rd cycle. This declined performance can be attributed to catalyst loss during the centrifugation recovery process between reuse cycles. It should be noted that, at the end of the 3rd cycle, the residual catalyst was collected by membrane filtration and its concentration was found about 300 mg/L, instead of 400 mg/L which was the initial catalyst loading at cycle 1. Lower catalyst loading means fewer active sites for the photogeneration of oxidising species and therefore lower solute degradation, thus explaining the above result. Another possible explanation might be the depletion of TiO_2 active sites by residual unreacted SAC molecules, reaction by-products or intermediates and thus less available active sites for photocatalytic oxidation [18, 30, 31]. Nevertheless, loss of catalytic activity does not take place in this case, since the obtained 70%, at cycle 3, is the expected SAC removal percentage in the presence of 300 mg/L ANA, based on results shown in section 3.4, which are also presented in the inset graph of Figure 7. This was expected since, the initial SAC concentration of 5 mg/L is a low adsorbate concentration that cannot significantly affect the formation of free radicals and other reactive oxidative species (ROS) on catalyst surface [32]. Moreover, Fernández-Ibáñez et al. (2003) have used a similar methodology for catalyst recovery and they reported that there is no TiO2 deactivation, when TiO2 reuse follows its separation from the reactant solution [33].

Furthermore, additional catalyst reuse experiments were performed with the catalyst being subjected to ultrasound cleaning (US) before its further use, in order to determine the impact of US on catalyst activity (Figure 7). It is well-known that US can remove impurities from the surface of heterogeneous metal catalysts, such as TiO_2, and can bring the reactant materials into more intimate contact with the catalyst surface, thus resulting in increased reaction

rates. Also, US assists catalyst dispersion and emulsification and can, therefore, increase the available contact surface area, which enhances chemical reactions between the components of the emulsion [34]. In this case, it is clear in Figure 7 that US did not improve the process efficiency. SAC removal remained unchanged at 81% and 84% during the 1st and 2nd reuse cycles, respectively, while the removal at the 3rd cycle was decreased about 4% compared to the respective experiments in the absence of US. This indicates that photocatalytic degradation mainly takes place through free radical and other reactive oxidative species (ROS) reactions and that catalyst agglomeration, as well as the presence of unreacted SAC molecules and by-products on the catalyst surface, was not a limiting factor in the system under study. Also, the negligible effect of US can be attributed to catalyst loss, which was greater than in the absence of US, between reuse cycles. After the end of the 3rd reuse cycle, the residual catalyst concentration was estimated at about 200 mg/L (i.e. 100 mg/L less than the residual catalyst in the corresponding experiment without US; the degree of agglomeration may be reduced by fracture in an ultrasonic field [34] and thus higher amounts of catalyst are lost through centrifugation and membrane filtration).

Figure 7

4 Conclusions

The photocatalytic treatment of saccharin (SAC), an emerging persistent contaminant, and bisphenol-A (BPA), a well-known endocrine disruptor, was studied. In this direction, interfaced anatase–rutile photocatalysts were produced by thermohydrolysis in the presence of small amounts (< 1%) of Sn(IV), which act as a rutile phase promoter. The activity of these catalysts was evaluated in terms of SAC and BPA degradation. Furthermore, the effect of operating conditions, such as initial solute concentration, catalyst type, loading and reuse, on photocatalytic performance was assessed and the conclusions drawn are summarised as follows:

- The photocatalytic efficiency of all novel TiO_2 nanocomposites was very similar in terms of SAC or BPA degradation. Factors that affected mostly the process performance were the initial organics concentration and the catalyst loading. Reaction rate constants increased when the initial solute concentration was decreased and when catalyst concentration was increased up to 400 mg/L. A further increase to 600 mg/L did not improve BPA degradation due to masking effects ascribed to excessive catalyst particles. TOC measurements revealed the presence of transformation products after the end of treatment, thus indicating the need for eco-toxicity estimation before any further scaling-up of the process.

- The recycled catalyst was used in three successive cycles without losing much of its efficiency and thus yielded 70% SAC removal at the end of the 3rd cycle. Finally, ultrasound cleaning of the reactant mixture, at the beginning of each reuse cycle, was applied, in additional experimental runs, and was revealed to have no effect on treatment efficiency.

References

[1] Z.-h. Liu, Y. Kanjo, S. Mizutani, Removal mechanisms for endocrine disrupting compounds (EDCs) in wastewater treatment — physical means, biodegradation, and chemical advanced oxidation: A review, Science of The Total Environment, 407 (2009) 731-748.

[2] V. Koutantou, M. Kostadima, E. Chatzisymeon, Z. Frontistis, V. Binas, D. Venieri, D. Mantzavinos, Solar photocatalytic decomposition of estrogens over immobilized zinc oxide, Catalysis Today, 209 (2013) 66-73.

[3] Z. Sang, Y. Jiang, Y.-K. Tsoi, K.S.-Y. Leung, Evaluating the environmental impact of artificial sweeteners: A study of their distributions, photodegradation and toxicities, Water Research, 52 (2014) 260-274.

[4] J. Tijani, O. Fatoba, L.F. Petrik, A Review of Pharmaceuticals and Endocrine-Disrupting Compounds: Sources, Effects, Removal, and Detections, Water Air Soil Pollut, 224 (2013) 1-29.

[5] J.-C. Sin, S.-M. Lam, A.R. Mohamed, K.-T. Lee, Degrading Endocrine Disrupting Chemicals from Wastewater by TiO2 Photocatalysis: A Review, International Journal of Photoenergy, 2012 (2012).

[6] M.R. Weihrauch, V. Diehl, Artificial sweeteners—do they bear a carcinogenic risk?, Annals of Oncology, 15 (2004) 1460-1465.

[7] A. Zygler, A. Wasik, J. Namieśnik, Analytical methodologies for determination of artificial sweeteners in foodstuffs, TrAC Trends in Analytical Chemistry, 28 (2009) 1082-1102.

[8] M. Scheurer, H.-J. Brauch, F.T. Lange, Analysis and occurrence of seven artificial sweeteners in German waste water and surface water and in soil aquifer treatment (SAT), Analytical and Bioanalytical Chemistry, 394 (2009) 1585-1594.

339 [9] F.T. Lange, M. Scheurer, H.-J. Brauch, Artificial sweeteners—a recently recognized class of emerging
340 environmental contaminants: a review, Analytical and Bioanalytical Chemistry, 403 (2012) 2503-2518.

341 [10] D.R. Van Stempvoort, J.W. Roy, S.J. Brown, G. Bickerton, Artificial sweeteners as potential tracers in
342 groundwater in urban environments, Journal of Hydrology, 401 (2011) 126-133.

343 [11] M. Scheurer, F.R. Storck, H.-J. Brauch, F.T. Lange, Performance of conventional multi-barrier drinking water
344 treatment plants for the removal of four artificial sweeteners, Water Research, 44 (2010) 3573-3584.

345 [12] P. Calza, V.A. Sakkas, C. Medana, A.D. Vlachou, F. Dal Bello, T.A. Albanis, Chemometric assessment and
346 investigation of mechanism involved in photo-Fenton and TiO2 photocatalytic degradation of the artificial
347 sweetener sucralose in aqueous media, Applied Catalysis B: Environmental, 129 (2013) 71-79.

348 [13] A.J. Li, O.J. Schmitz, S. Stephan, C. Lenzen, P.Y.-K. Yue, K. Li, H. Li, K.S.-Y. Leung, Photocatalytic
349 transformation of acesulfame: Transformation products identification and embryotoxicity study, Water Research,
350 89 (2016) 68-75.

351 [14] S. Malato, P. Fernández-Ibáñez, M.I. Maldonado, J. Blanco, W. Gernjak, Decontamination and disinfection
352 of water by solar photocatalysis: Recent overview and trends, Catalysis Today, 147 (2009) 1-59.

353 [15] Y. Zhang, J.L. Zhou, Occurrence and removal of endocrine disrupting chemicals in wastewater,
354 Chemosphere, 73 (2008) 848-853.

355 [16] J.-M. Herrmann, Heterogeneous photocatalysis: fundamentals and applications to the removal of various
356 types of aqueous pollutants, Catalysis Today, 53 (1999) 115-129.

357 [17] N.P. Xekoukoulotakis, C. Drosou, C. Brebou, E. Chatzisymeon, E. Hapeshi, D. Fatta-Kassinos, D.
358 Mantzavinos, Kinetics of UV-A/TiO2 photocatalytic degradation and mineralization of the antibiotic
359 sulfamethoxazole in aqueous matrices, Catalysis Today, 161 (2011) 163-168.

360 [18] E. Chatzisymeon, E. Stypas, S. Bousios, N.P. Xekoukoulotakis, D. Mantzavinos, Photocatalytic treatment of
361 black table olive processing wastewater, Journal of Hazardous Materials, 154 (2008) 1090-1097.

362 [19] A. Pichavant, E. Provost, M.-H. Berger, W. Fürst, J.-F. Hochepied, Interfaced titanium dioxide anatase–rutile
363 nanocomposites by thermohydrolysis in presence of small amounts of Sn(IV) and their photocatalytic properties,
364 Colloids and Surfaces A: Physicochemical and Engineering Aspects, 462 (2014) 64-68.

365 [20] G. F. Ferreira, M. G. Maniero, J. R. Guimarães, Degradation of Sucralose by Peroxidation Assisted with
366 Ultraviolet Radiation and Photo-Fenton, International Journal of Engineering and Technology, 7 (2015) 438-444.

367 [21] S.W. Chen, W.C. Li, Z.G. Sun, H.Y. Xie, Degradation of Artificial Sweetener Saccharin Sodium by Advanced
368 Oxidation Technology, Applied Mechanics and Materials, 448-453 (2014) 7-10.

369 [22] A.A. Gribb, J.F. Banfield, Particle size effects on transformation kinetics and phase stability in
370 nanocrystalline TiO2, American Mineralogist, 82 (1997) 717-728.

371 [23] S.L. Murov, I. Carmichael, G.L. Hug, Handbook of Photochemistry, Second Edition, Taylor & Francis1993.

372 [24] I. Trandafir, V. Nour, M.E. Ionică, Development and validation of an HPLC methods for simulatneous
373 quantification of acesulfame-K, saccharin, aspartame, caffeine and benzoic acid in cola soft drinks, Scientific
374 Study & Research X(2009) 185-194.

375 [25] V.M. Daskalaki, Z. Frontistis, D. Mantzavinos, A. Katsaounis, Solar light-induced degradation of bisphenol-A
376 with TiO2 immobilized on Ti, Catalysis Today, 161 (2011) 110-114.

[26] F. Fresno, D. Tudela, J.M. Coronado, J. Soria, Synthesis of Ti1−xSnxO2 nanosized photocatalysts in reverse microemulsions, Catalysis Today, 143 (2009) 230-236.

[27] A.R. Khataee, M.N. Pons, O. Zahraa, Photocatalytic degradation of three azo dyes using immobilized TiO2 nanoparticles on glass plates activated by UV light irradiation: Influence of dye molecular structure, Journal of Hazardous Materials, 168 (2009) 451-457.

[28] A.O. Kondrakov, A.N. Ignatev, F.H. Frimmel, S. Bräse, H. Horn, A.I. Revelsky, Formation of genotoxic quinones during bisphenol A degradation by TiO2 photocatalysis and UV photolysis: A comparative study, Applied Catalysis B: Environmental, 160–161 (2014) 106-114.

[29] N. Miranda-García, S. Suárez, M.I. Maldonado, S. Malato, B. Sánchez, Regeneration approaches for TiO2 immobilized photocatalyst used in the elimination of emerging contaminants in water, Catalysis Today, 230 (2014) 27-34.

[30] M. Argyle, C. Bartholomew, Heterogeneous Catalyst Deactivation and Regeneration: A Review, Catalysts, 5 (2015) 145.

[31] S. Salaeh, M. Kovacic, D. Kosir, H. Kusic, U. Lavrencic Stangar, D.D. Dionysiou, A. Loncaric Bozic, Reuse of TiO2-based catalyst for solar driven water treatment; thermal and chemical reactivation, Journal of Photochemistry and Photobiology A: Chemistry, 333 (2017) 117-129.

[32] J. Araña, E. Tello Rendón, J.M. Doña Rodríguez, J.A. Herrera Melián, O. González Díaz, J. Pérez Peña, High concentrated phenol and 1,2-propylene glycol water solutions treatment by photocatalysis: Catalyst recovery and re-use, Applied Catalysis B: Environmental, 30 (2001) 1-10.

[33] P. Fernández-Ibáñez, J. Blanco, S. Malato, F.J.d.l. Nieves, Application of the colloidal stability of TiO2 particles for recovery and reuse in solar photocatalysis, Water Research, 37 (2003) 3180-3188.

[34] D. Ensminger, Ultrasonics: Fundamentals, Technology, Applications, Second Edition, Revised and Expanded, 1988.

List of Figures

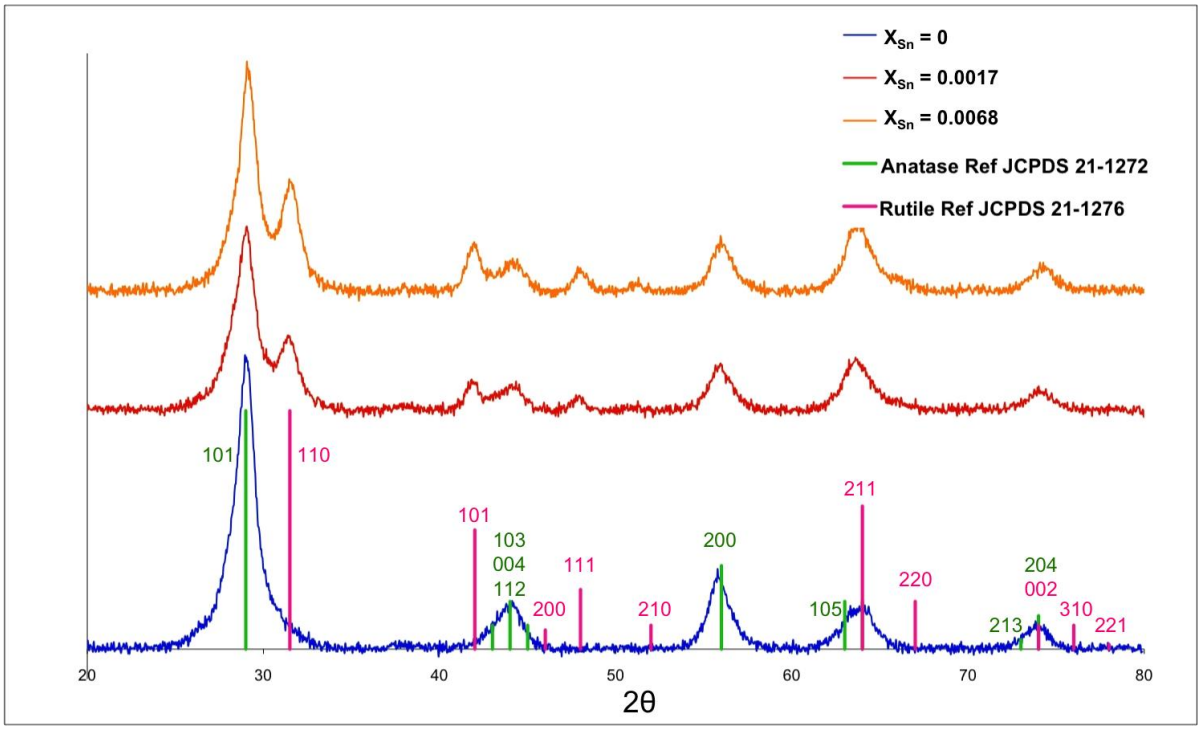

421

422 Figure 1

423

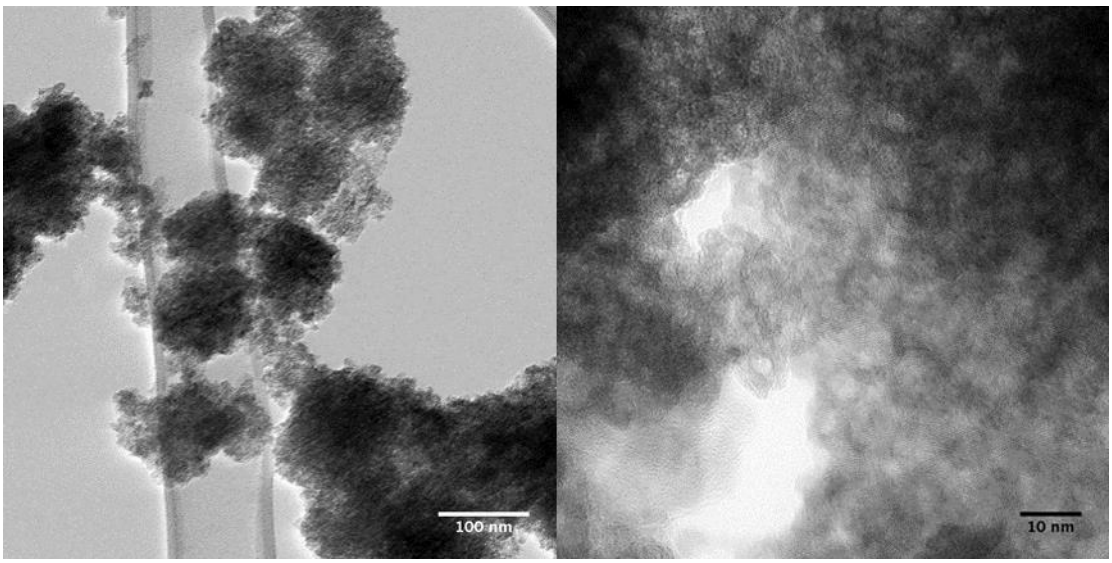

424

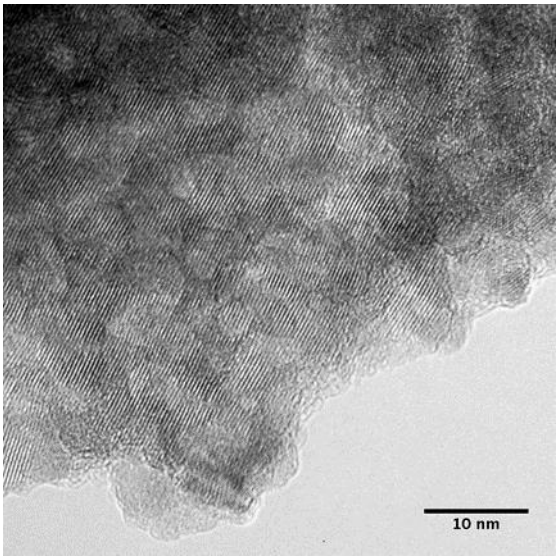

425

426 Figure 2

427

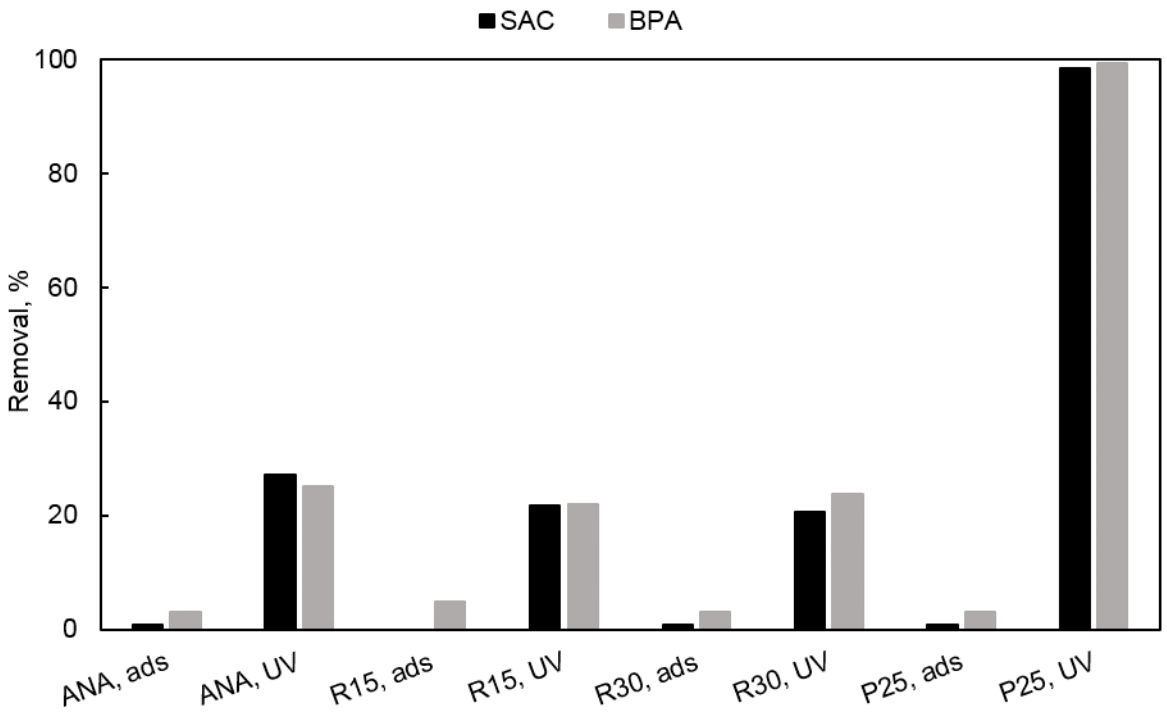

428

429 Figure 3

430

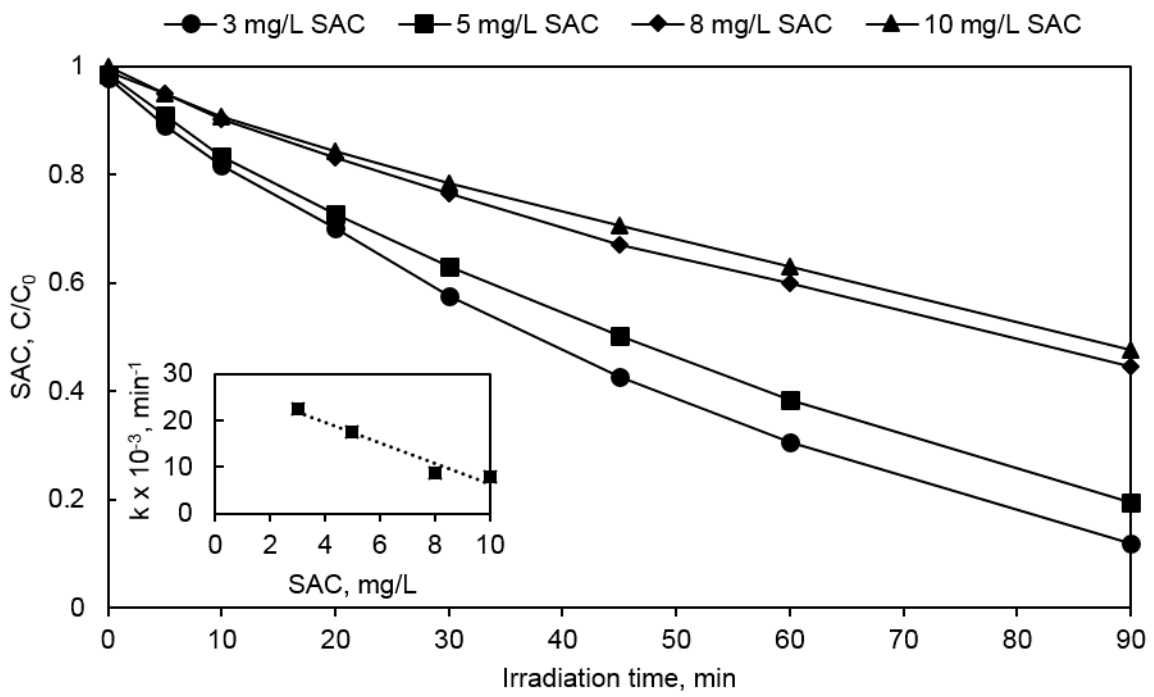

431

432 Figure 4

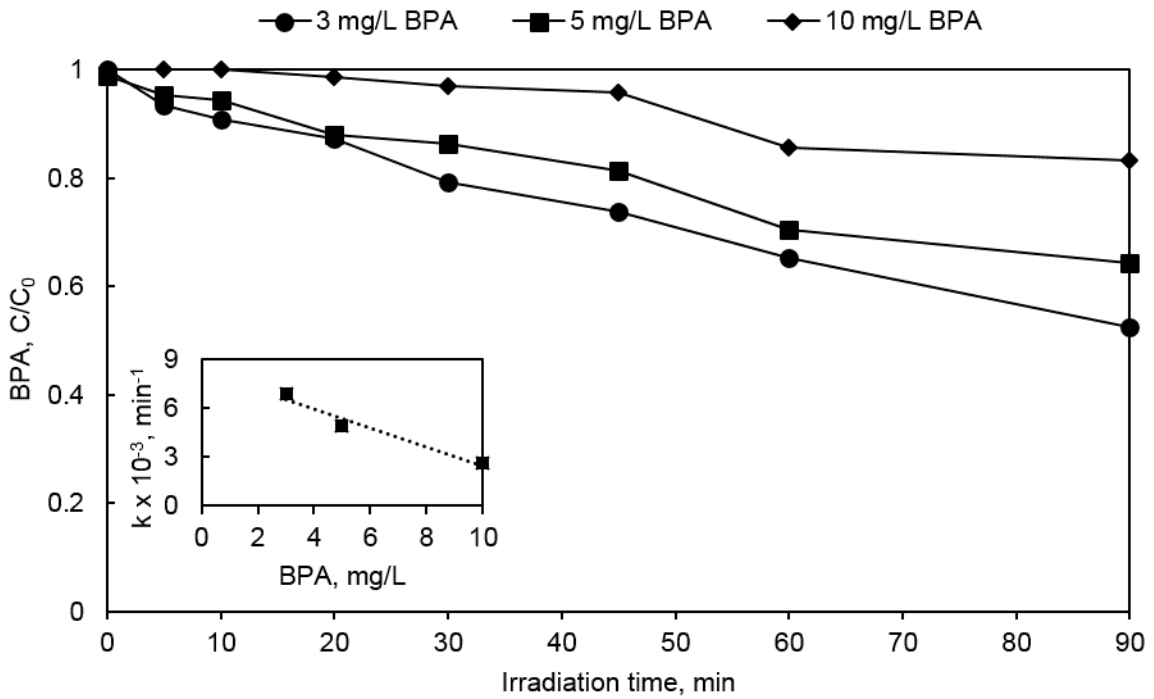

433

434 Figure 5

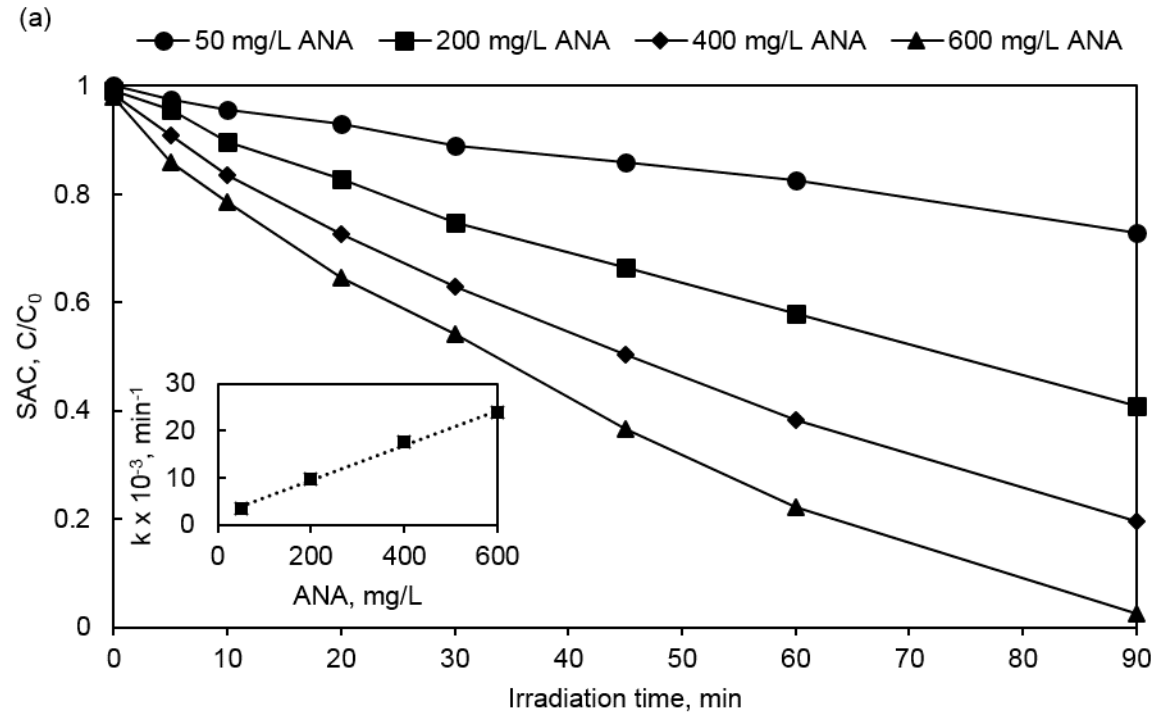

435

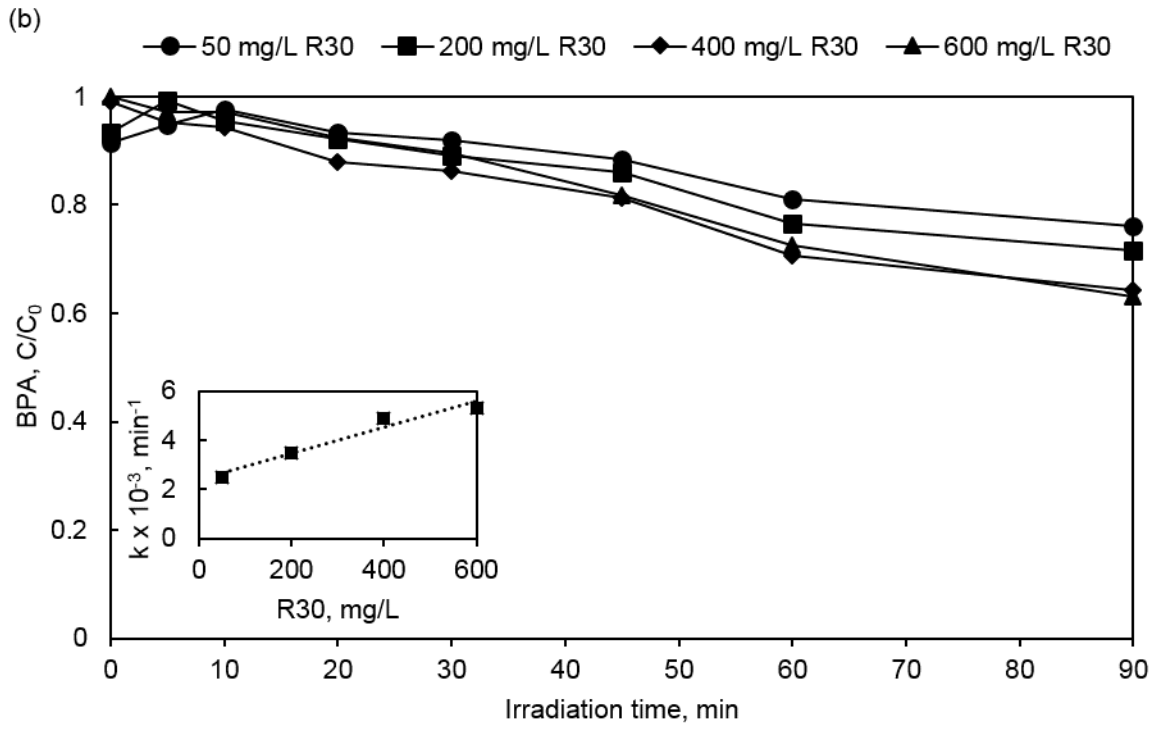

436

437 Figure 6

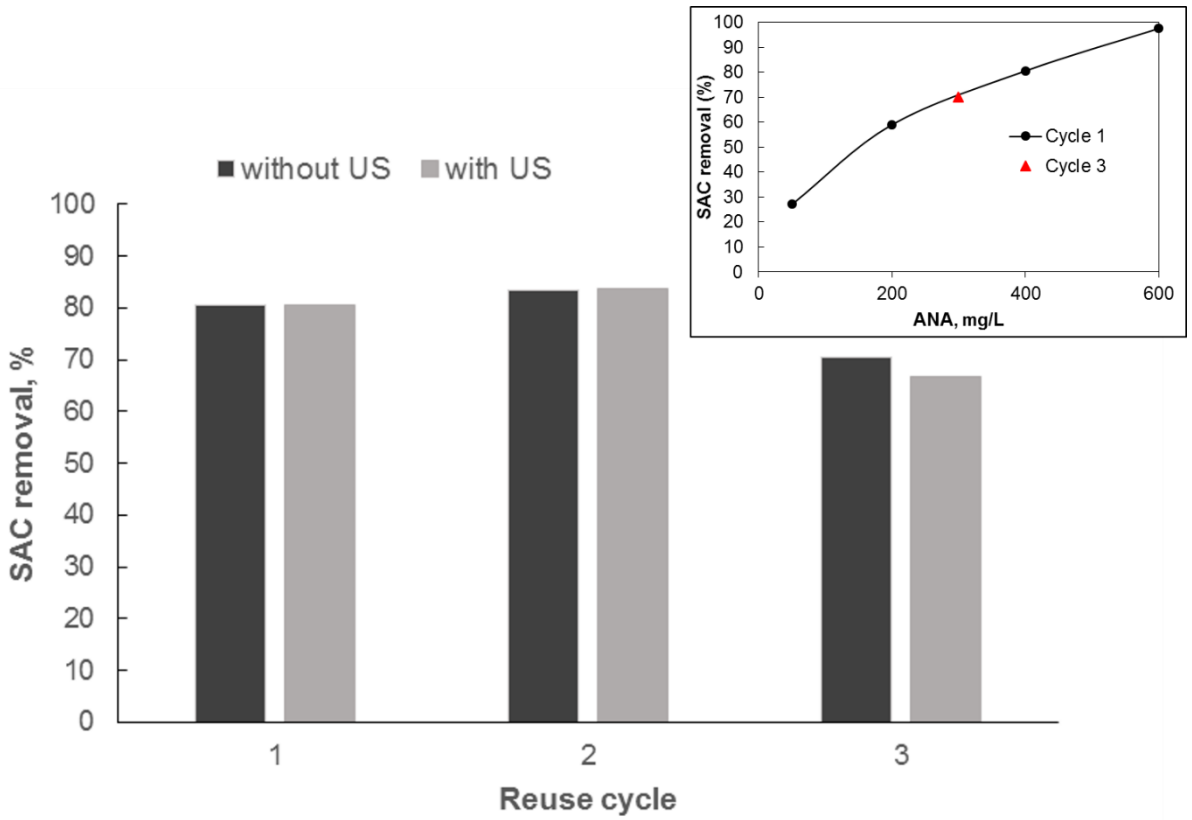

438

439 Figure 7

440

441

442